CARBON 49 (2011) 24–36

available at www.sciencedirect.com

ScienceDirect

journal homepage: www.elsevier.com/locate/carbon

Surface and structural characterization of multi-walled carbon nanotubes following different oxidative treatments

Kevin A. Wepasnick [a], Billy A. Smith [a], Kaitlin E. Schrote [b], Hannah K. Wilson [c], Stephen R. Diegelmann [a,d], D. Howard Fairbrother [a,d,e,*]

[a] Department of Chemistry, Johns Hopkins University, 3400 North Charles Street, Baltimore, MD 21218, United States
[b] Department of Chemistry, College of Notre Dame of Maryland, 4701 North Charles Street, Baltimore, MD 21210, United States
[c] Department of Chemical and Biochemical Engineering, University of Maryland, Baltimore County, 1000 Hilltop Circle, Baltimore, MD 21250, United States
[d] Institute for NanoBioTechnology, Johns Hopkins University, 3400 North Charles Street, Baltimore, MD 21218, United States
[e] Department of Materials Science and Engineering, Johns Hopkins University, 3400 North Charles Street, Baltimore, MD 21218, United States

ARTICLE INFO

Article history:
Received 28 May 2010
Accepted 13 August 2010
Available online 18 August 2010

ABSTRACT

Six commonly used wet chemical oxidants (HNO_3, $KMnO_4$, H_2SO_4/HNO_3, $(NH_4)_2S_2O_8$, H_2O_2, and O_3) were evaluated in terms of their effects on the surface chemistry and structure of MWCNTs using a combination of analytical techniques. X-ray photoelectron spectroscopy (XPS) and energy dispersive spectroscopy (EDX) were used to characterize the extent of surface oxidation, while chemical derivatization techniques used in conjunction with XPS allowed the concentration of carboxyl, carbonyl, and hydroxyl groups at the surface to be quantified for each MWCNT sample. Our results indicate that the distribution of oxygen-containing functional groups was insensitive to the reaction conditions (e.g., w/w% of oxidant), but was sensitive to the identity of the oxidant. MWCNTs treated with $(NH_4)_2S_2O_8$, H_2O_2, and O_3 yielded higher concentrations of carbonyl and hydroxyl functional groups, while more aggressive oxidants (e.g., HNO_3, $KMnO_4$) formed higher fractional concentrations of carboxyl groups. IR spectroscopy was unable to identify oxygen-containing functional groups present on MWCNTs, while Raman spectra highlighted the frequently ambiguous nature of this technique for measuring CNT structural integrity. TEM was able to provide detailed structural information on oxidized MWCNT, including the extent of sidewall damage for different oxidative treatments.

© 2010 Elsevier Ltd. All rights reserved.

1. Introduction

Carbon nanotubes (CNTs) have enormous commercial potential in applications including polymer composites [1] and biomedical applications [2]. To be useful in these applications, it is necessary to overcome the CNTs' extreme hydrophobicity which leads to aggregation in polar liquids [3,4]. To improve the CNT's hydrophilicity, their surfaces are often tailored by covalent or non-covalent modification strategies. Covalent surface modification involves the incorporation of hydrophilic substituents into the exterior CNT sidewalls [5]. In contrast, non-covalent surface modification involves adsorption of a surfactant (e.g., NaDDBS [6]) onto the CNT so that properties can be tailored without affecting the intrinsic CNT structure [7]. Both covalent and non-covalent modification strategies have been used to prepare CNTs for consumer

* *Corresponding author at*: Department of Chemistry, Johns Hopkins University, 3400 North Charles Street, Baltimore, MD 21218, United States. Fax: +1 410 516 8420.
E-mail address: howardf@jhu.edu (D.H. Fairbrother).
0008-6223/$ - see front matter © 2010 Elsevier Ltd. All rights reserved.
doi:10.1016/j.carbon.2010.08.034

Samsung Ex. 1010, Page 1 of 13
Samsung Electronics Co., Ltd., et al. v. Molecular Rebar Design, LLC
IPR2025-00356

applications [7–10]. For example, the surface of CNTs used in reinforced polymer composites are often modified covalently by the addition of polar functional groups, not only to improve dispersion properties but also to enhance chemical interactions with the resin matrix [1,3,4,11].

Among the various types of covalent surface modification strategies, deliberately grafting oxygen-containing functional groups at the open ends and sidewalls of CNTs is a popular and versatile approach [5]. Indeed, this strategy is often used to create CNTs that disperse in water [12–14]. Surface oxidation can also occur unintentionally after CNTs are released into the environment, either through exposure to natural oxidizing agents such as ozone and hydroxyl radicals [15,16], or as a result of common water treatment processes that employ UV irradiation and ozonolysis [17,18].

The deliberate incorporation of surface oxygen into CNTs has been achieved through a variety of methods, chiefly wet chemical oxidation [14,19–21], plasma treatments [22,23], and rational functionalization strategies involving synthetic organic chemistry [24]. Among these various treatment methods, wet chemical techniques using different oxidizing acids (e.g., HNO_3) and strong oxidants (e.g., O_3) tend to be the most prevalent due to their easy implementation in laboratory and industrial settings. These same oxidative treatments are also used to help remove amorphous carbon and metallic impurities from as-produced CNTs [25–27]. Despite the fact that a wide variety of oxidizing conditions (defined by the oxidant and the reaction conditions) are used to treat and modify CNTs, the rationale behind the choice of a particular set of oxidizing conditions is rarely discussed, with few exceptions [28]. Furthermore, the effect of different oxidizing conditions on CNT surface chemistry or structure is seldom considered.

Different oxidizing conditions are likely to affect both the concentration of oxygen atoms incorporated into the CNTs and the distribution of oxygen-containing functional groups. The importance of determining both of these parameters can be appreciated by considering the effect that surface chemistry exerts on a number of important properties. For example, surface oxidation has been shown to exert a pronounced effect on both the sorption properties and colloidal stability of CNTs [12,13,29,30]. Obtaining more detailed information on the effect that different oxidizing conditions have on the distribution of oxygen-containing functional groups will be important in optimizing the structure and function of more complex nanostructures, where CNT oxidation is often the first step. In functionalization strategies, the role of oxidation is to create "foothold" functional groups, such as carboxyl groups, which then serve as attachment points to anchor either larger biomolecular structures [31,32] or nanoparticles [19,28–32]. In rational functionalization strategies used to modify CNT surface chemistry, oxygen-containing functional groups are often subjected to chemical transformations; for example, COOH groups are transformed to acid chlorides as a route to create aminated CNTs [24]. Consequently, knowledge of the concentration and distribution of different oxygen functional groups on the CNT surface following wet chemical oxidative treatments would allow researchers to better control the ultimate structure and properties of the CNT-based materials.

One popular analytical method used to quantify the extent (or level) of surface oxidation following different oxidative treatments is X-ray photoelectron spectroscopy (XPS) [5,12,13,30]. With this technique, the distribution of oxygen-containing functional groups (e.g., C—O, C=O and O—C=O) is also often characterized by deconvoluting the C(1s) spectral envelope to obtain quantitative information, based on differences in binding energies [19]. However, the C(1s) spectral envelope is typically broad and featureless due to both the proximity of the binding energies associated with different oxygen-containing functional groups and the limited resolution of typical energy analyzers [5,33]. Furthermore, the presence of the π–π^* shake-up feature in materials such as CNTs with delocalized π-electron systems causes further congestion in the C(1s) region [5]. Consequently, peak-fitting the C(1s) region typically leads to misleading and ambiguous results in terms of the calculated distribution of oxygen-containing functional groups.

To overcome the limitations inherent in XPS peak-fitting, derivatization methods have been developed to characterize certain key oxygen-containing functional groups on plasma-treated polymer surfaces [34], and more recently on carbonaceous surfaces such as CNTs [23,30,35]. In these applications of chemical derivatization, a targeted oxygen-containing functional group reacts selectively with a specific derivatizing reagent that contains a unique chemical tag (e.g., fluorine atoms). After each derivatization reaction, the concentration of the chemical tags can be quantified, allowing the concentration of the targeted functional group to be determined. Chemical derivatization methods for quantifying the distribution of oxygen-containing functional groups on CNTs have been used in several recent studies. For example, Zschoerper et al. have used chemical derivatization reactions utilizing fluorine tags in conjunction with XPS to show that Ar/O_2 and Ar/H_2O plasma treatment conditions (e.g., pressure, time) affect the distribution of oxygen-containing functional groups on SWCNTs and MWCNTs, primarily increasing the C=O functional groups [23]. In another type of chemical derivatization study, Masheter et al. derivatized COOH functional groups using a two-step method in which carboxyl groups were converted to an acid chloride and subsequently reacted with 4-nitrophenol to yield a nitro group. Analysis of the N(1s) region by XPS was then used to measure increases in the COOH group concentration of SWCNTs and MWCNTs after H_2SO_4/HNO_3 treatment [36]. The florescent labeling of oxygen-containing functional groups is another method of chemical derivatization that has been developed to examine oxidized CNTs. In this method, carboxyl, hydroxyl and carbonyl surface species are labeled with fluorescent tags [35]. Dementev et al., used this technique to determine the increase in COOH, C=O and C—OH group concentrations for commercially available HCl and HNO_3 treated SWCNTs. Results from these studies indicated that the carbonyl functional groups showed the greatest increase in concentration compared to the untreated material [35].

In this work, we have performed a systematic study of the effect that different oxidants and reaction conditions have on the surface chemistry and structure of MWCNTs. Specifically, the effects of six wet chemical oxidants (HNO_3 [13], H_2SO_4/HNO_3 [37], $KMnO_4$ [38], H_2O_2 [39], O_3 [40], and $(NH_4)_2S_2O_8$

Samsung Ex. 1010, Page 2 of 13
Samsung Electronics Co., Ltd., et al. v. Molecular Rebar Design, LLC
IPR2025-00356

[41]) used under different reaction conditions (e.g., w/w%) were examined. Our decision to focus on MWCNTs was based on the fact that they are less expensive to manufacture and, thus, more often incorporated into large scale commercial applications [11]. We also deliberately selected a single source of MWCNTs, allowing us to directly compare and contrast the effect of different oxidizing conditions on a common starting material. Changes in surface chemistry were studied using a combination of infrared (IR) spectroscopy, energy dispersive X-ray spectroscopy (EDX), XPS, and chemical derivatization. In addition to changes in surface chemistry, we also evaluated the effects of different oxidizing conditions on the MWCNT structure, using transmission electron microscopy (TEM) and Raman spectroscopy.

2. Experimental

2.1. Materials

MWCNTs (outer diameters 15 ± 5 nm, lengths 5–20 μm, 95% by TGA, PD15L520-21408) were purchased from Nanolab, Inc. (Newton, MA) and used as received. Poly(acrylic acid) (PAA) and benzoic acid (BA) were purchased from Sigma–Aldrich. Poly(4-vinyl benzoic acid) (PBA) was purchased from Polymer Source, Inc. Polyethyleneterphalate (PET) and polyethylene (PE) were purchased from Goodfellow. Derivatizing reagents: 2,2,2-trifluoroacetic anhydride (TFAA), 2,2,2-trifluoroethanol (TFE), N,N′-di-*tert*-butyl-carbodiimide (DTBC), and 2,2,2-trifluoroethylhydrazine (TFH) were purchased from Sigma–Aldrich and used as received. All reagents were 99% pure, with the exception of TFH, which was obtained as a 70% solution (by volume) in water.

2.2. Wet chemical treatments

The experimental details of each wet chemical treatment were based upon established procedures used to either oxidize or purify CNTs [13,27,37–41]. At the conclusion of the oxidation process, excess oxidizing agents, dissolved salts, and reaction byproducts were removed by centrifugation, followed by repeated washing, decanting and further centrifugation of the CNTs in fresh Milli-Q water until the resistance of the supernatant exceeded 500 kΩ. At this stage, the residual acid or electrolyte concentration was deemed to be negligible. In the final step, the solution was evaporated by heating to 100 °C and the MWCNT powder was ball milled for 15 min. The ball milled samples were then stored in glass vials until surface or structural analysis was performed.

In the following text, we outline details specific to each oxidative method. However, it should be noted that in some cases, the reaction conditions for a particular oxidant were varied by using different ratios of oxidants to MWCNT. (i) **HNO_3** [13]. MWCNTs (100 mg) were sonicated (70 W, Branson-ic) in 200 mL of 10–70% w/w HNO_3 for 1 h. Typical literature methods for CNT purification and oxidation use 70% [13], but lower percentages have also been reported [27]. To affect oxidation, the MWCNT/HNO_3 mixture was refluxed for 1.5 h at 140 °C. (ii) **$KMnO_4$** [38]. $KMnO_4$ (87–250 mg) was dissolved in 200 mL of 0.5 M H_2SO_4. MWCNTs (100 mg) were sonicated in 200 mL of 0.5 M H_2SO_4 for 30 min. The MWCNT/H_2SO_4 mixture was then heated to 150 °C prior to the $KMnO_4$ solution being added dropwise. The resultant MWCNT/$KMnO_4$ mixture was then refluxed for 5 h at 150 °C. When the reaction had cooled to room temperature, 10 mL of concentrated HCl was added to dissolve the MnO_2 byproduct. (iii) **H_2O_2** [39]. MWCNTs (100 mg) were added to 15 mL of 30% H_2O_2 and the mixture heated to 70 °C for 4 days with continuous stirring. Every 24 h, 1–5 mL of 30% H_2O_2 was added to account for the volume lost to evaporation. (iv) **H_2SO_4/HNO_3** [37]. H_2SO_4 and HNO_3 were combined in a 3:1 ratio to create a solution with a final volume of 8 mL. MWCNTs (100 mg) were added to this solution and the mixture was heated to 70 °C for 8 h without stirring. (v) **O_3** [40]. MWCNTs (200 mg) were added to 200 mL of Milli-Q water, and the mixture was sonicated for 30 min. The gas phase effluent from an arc discharge O_3 source was then bubbled through the suspension for 1 h with vigorous stirring. The steady-state aqueous concentration of O_3 in solution was determined to be 12 mg/L as measured by a modified indigo colorimetric method [42]. (vi) **$(NH_4)_2S_2O_8$** [41]. MWCNTs (50 mg) were added to 50 mL of piranha solution (4:1 96% H_2SO_4:30% H_2O_2) at 80 °C. To the MWCNTs, 4–6 g of $(NH_4)_2S_2O_8$ dissolved in 50 mL of 96% H_2SO_4 was added and the resultant mixture stirred for 4 h. The reaction was then quenched by the addition of 250 mL iced Milli-Q water.

2.3. Surface analysis of oxidized MWCNTs

2.3.1. X-ray photoelectron spectroscopy (XPS)

For XPS analysis, a small quantity (~5 mg) of MWCNTs was dusted onto double sided copper tape ($1 \times 1\ cm^2$) such that no copper was visible. Samples were then loaded into a PHI 5400 XPS system ($P_{base} < 5 \times 10^{-9}$ Torr) and analyzed using Mg Kα X-rays (1253.6 eV). Ejected photoelectrons were measured with a precision high energy electron analyzer operating at constant pass-energy. Two sets of parameters were used for the scans depending on the information required: elemental quantification was performed using a pass-energy of 178.95 eV with a scan rate of 0.250 eV/step, while high-resolution scans of individual spectral envelopes were performed with a pass-energy of 44.75 eV and a scan rate 0.125 eV/step. XP spectra were processed with commercially available software (CasaXPS), and atomic concentrations were quantified by integration of the relevant photoelectron peaks.

2.3.2. Energy dispersive X-ray spectroscopy (EDX)

To prepare samples for EDX, a film (>50 μm) was created by pressing MWCNTs onto double sided copper tape. The samples were then placed into a JEOL JSM-6700F SEM and irradiated with a 10 keV electron beam. Compositional information on each MWCNT was acquired through EDX, using a Silicon SUTW-Sapphire EDAX detector to analyze the energy and relative intensity of emitted X-rays.

2.3.3. Chemical derivatization in conjunction with XPS analysis

Based on previously developed protocols [33,43], individual derivatizing reactions were performed using: (i) TFE (1.0 mL/pyridine (0.4 mL))/DTBC (0.2 mL) to quantify carboxylic

Samsung Ex. 1010, Page 3 of 13
Samsung Electronics Co., Ltd., et al. v. Molecular Rebar Design, LLC
IPR2025-00356

acid groups (COOH), (ii) TFAA (1.0 mL) to quantify hydroxyl groups (C—OH), and (iii) TFH (0.2 mL) to quantify carbonyl groups (C=O). Each derivatization reaction was carried out in a specially designed glass reaction vessel [33]. Two types of samples were used: 5 mg MWCNT powder or a $1 \times 1\ cm^2$ polymer substrate, the latter used in reference or control studies. For MWCNTs, separate 5-mg aliquots were used for each derivatization reaction. The MWCNT or polymer substrate was placed in a glass cup suspended within the reaction vessel. Once the sample had been placed in the cup, the liquid phase derivatization reagents were placed in the bottom of the reaction vessel in close spatial proximity (~2 cm) to the sample; our results have shown that this close physical proximity promoted the reaction efficiency. At this stage, the liquid phase derivatizing reagents were frozen with liquid nitrogen before the reaction vessel was evacuated to <10 mTorr and sealed. The reaction vessel was then allowed to thaw, filling the glass reaction vessel with vapor phase derivatizing reagents. Each derivatizing reaction was allowed to proceed for 18 h at room temperature. At the conclusion of each derivatization reaction, samples were removed from the sealed reaction vessel and promptly analyzed by XPS to quantify the surface composition.

2.3.3.1. Derivatization reactions.

2.3.3.1.1 TFE/DTBC As shown in Fig. 1, the reaction of TFE with carboxylic acid (COOH) groups, **1**, in the presence of DTBC can yield two surface products: the first is a trifluoroethyl ester, **4**, (containing a CF_3 group) whose formation releases the volatile 1,3-di-*tert*-butyl urea, **5**, as a byproduct; the second is a surface bound di-*tert*-butyl-N-acyl urea, **3**, containing two nitrogen atoms. Despite the popularity of carbodiimide activators in coupling reactions involving COOH groups in surface science [5,34,43] and organic synthesis [32,44], the nitrogen containing N-acyl urea has been largely ignored. However, evidence of N-acyl urea, **3**, formation has been observed in a number of coupling reactions between DTBC and carboxylic acid groups. For example, Nakajima and Ikada proposed that in the presence of excess DTBC, the N-acyl urea, **3**, is produced when the O-acyl isourea activated complex, **2**, that initially forms from the reaction of DTBC with carboxylic acid groups, undergoes an irreversible rearrangement [45]. Iwasawa et al. have suggested that the N-acyl urea, **3**, can also form by rearrangement of an O-acyl isourea activated complex, **2**, that is sterically hindered and inaccessible to nucleophilic attack [46]. As part of our present investigation, we performed an extensive set of experiments (detailed in Supporting Information) involving DTBC reactions with both MWCNT and polymer substrates. Results from these studies indicated that: (i) both reaction pathways detailed in Fig. 1 are possible, (ii) the N(1s) signal observed as a result of the TFE/DTBC reaction with MWNCTs is principally due to the formation of an N-acyl urea, and (iii) although the trifluoroethyl ester, **4**, is the dominant product, both the N(1s) and F(1s) signals must be considered to accurately quantify the concentration of COOH groups present.

2.3.3.1.2 TFAA As shown in Fig. 2, TFAA reacts selectively with hydroxyl (C—OH) groups to form a trifluoromethyl ester group and expels trifluoroacetic acid as a byproduct. This reaction has been previously studied using reference polymers in our research group and proceeds with high selectivity and efficiency [33].

2.3.3.1.3 TFH As shown in Fig. 3, the reaction of carbonyl (C=O) groups with TFH produces one exclusive surface product, a trifluorinated hydrazone, where the terminal nitrogen group in TFH forms a double bond with the carbonyl (C=O) carbon, and oxygen is expelled as H_2O. This reaction has been studied previously in our research group on reference polymers and proceeds with high selectivity and efficiency towards C=O groups [33].

2.3.3.2 Determining the extent of non-specific binding In any derivatizing reaction, non-specific binding of the derivatization reagents with the substrate (i.e., *via* physisorption) is possible. Under these circumstances, spectroscopic signatures of derivatization products (in the present case, F(1s) and N(1s) signals) would cause an overestimation of the functional group concentration. To quantify the extent of non-specific binding, a series of derivatization reactions were conducted on MWCNTs that had been thermally heat-treated (1800 °C for 12 h under vacuum) to remove essentially all of their surface oxygen functional groups (≈1% oxygen as measured by XPS). The fluorine and nitrogen atomic concentrations measured on these heat-treated MWCNTs (⩽0.5% for both fluorine and nitrogen) were used to quantify the extent non-specific binding. These quantities served as baseline values and were subtracted from all fluorine and nitrogen atomic concentrations measured on the MWCNTs studied in this investigation, following each derivatization reaction.

2.3.3.3 Quantifying functional group concentrations As shown in Figs. 1–3, derivatization reactions yield specific surface products with known stoichiometries. From the measured C(1s), F(1s), and N(1s) XPS peak areas measured before and after each derivatization reaction, as well as the oxygen XPS peak area prior to derivatization, it is possible to calculate the surface concentration of oxygen atoms contained in COOH ($[O]_{COOH}$), C—OH ($[O]_{OH}$), and C=O ($[O]_{C=O}$) groups at the MWCNT surface. The advantage of this approach is that it does not require the O(1s) XPS peak area to be measured after each derivatization reaction, which often exhibit non-systematic variations, probably due to water adsorption. The validity of ignoring the O(1s) signal after derivatizing reactions was verified by using this approach with reference polymers and calculating the correct concentration of functional groups. Thus, in the following sections, [F], [N] and [C] refer to the atomic concentrations of these three elements determined after each derivatization reaction, ignoring the O(1s) XPS signal.

2.3.3.3.1 Carboxyl groups Based on the stoichiometries of the two possible reaction products shown in Fig. 1, an analytical expression for the $[O]_{COOH}$ can be derived using [F] and [N] values measured after the TFE/DTBC reaction, along with the atomic concentration of carbon ($[C_0]$) measured prior to the derivatization reaction:

Samsung Ex. 1010, Page 4 of 13
Samsung Electronics Co., Ltd., et al. v. Molecular Rebar Design, LLC
IPR2025-00356

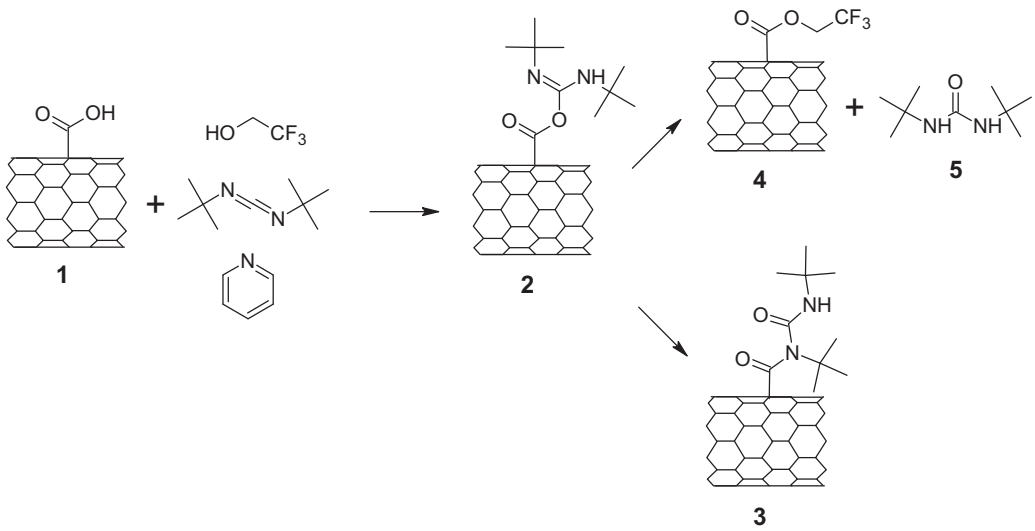

Fig. 1 – The selective reaction of carboxyl (COOH) groups, 1, with DTBC to form an O-acyl isourea intermediate, 2. Subsequent decomposition of the intermediate can produce either the fluorinated ester, 4, or the N-acyl urea, 3.

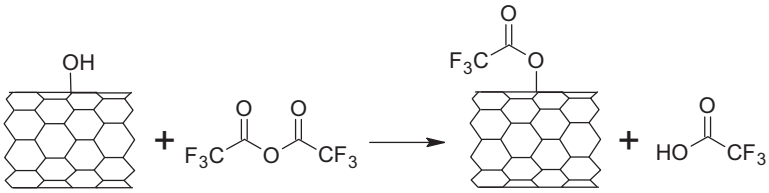

Fig. 2 – The selective reaction of hydroxyl (OH) groups with trifluoroacetic anhydride (TFAA) to form a fluorinated ester.

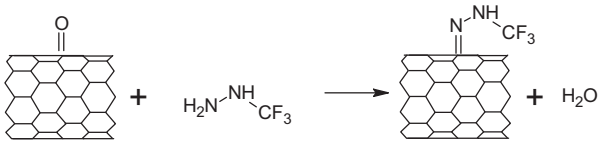

Fig. 3 – The selective reaction of carbonyl (C=O) groups with trifluoroethylhydrazine (TFH) to form a fluorinated hydrazone.

$$[O]_{COOH} = \frac{6[N][C_0]}{\varepsilon_N(6 \quad 10[F] \quad 33[N])} + \frac{4[F][C_0]}{\varepsilon_F(6 \quad 10[F] \quad 33[N])} \tag{1}$$

The derivation for Eq. (1) is outlined in the Supporting information.

It is important to note that there are two oxygen atoms for each COOH group and the values we report are for the atomic oxygen concentration, $[O]_{COOH}$, rather than the functional group concentration, [COOH]. The equation for the TFE/DTBC reaction has two efficiency factors, ε_F and ε_N, that correspond to the efficiency of the two possible reaction pathways that lead to fluorine and nitrogen incorporation, respectively. To test the ability of Eq. (1) to quantify $[O]_{COOH}$, [F] and [N] were measured on a COOH-containing reference polymer, polybenzoic acid (PBA – $(–CH_2CH–(C_6H_4COOH))_n$) following derivatization with TFE/DTBC. Data from these experiments revealed a surface composition of 18.5%F and 1.3%N. Using Eq. (1) and $\varepsilon_F = \varepsilon_N = 1$ resulted in a value of $[O]_{COOH}$ = 17.8% which is 98% of the expected value (18.2%). This supports the idea that $\varepsilon_F = \varepsilon_N = 1$ is correct. It should also be noted that if only [F] is used, a value of $[O]_{COOH}$ = 14.5% is calculated (80% of the expected value). This further supports the idea that both fluorine and nitrogen XPS signals are needed to accurately quantify $[O]_{COOH}$.

Eq. (1) can also be used on substrates that contain COOH groups, but where no nitrogen XPS signal was observed after reaction with TFE/DTBC, such as polyacrylic acid (PAA – $(–CH_2CH–(COOH))_n$). Thus, for PAA, the atomic concentration of fluorine was 37.7%, and if we apply Eq. (1) using $\varepsilon_F = \varepsilon_N = 1$, a value of $[O]_{COOH}$ = 42.7% is obtained, 107% of the expected value (40%). This is identical to the value obtained when the possibility of N-acyl urea formation was excluded, demonstrating that Eq. (1) can be applied whether or not a nitrogen XPS signal is observed.

2.3.3.3.2 *Hydroxyl groups* For the TFAA reaction, the atomic concentration of fluorine measured after derivatization ([F]) and the initial atomic concentration of carbon ($[C_0]$) are sufficient to calculate the original concentration of C–OH groups present at the surface, using Eq. (2) [33]:

$$[O]_{OH} = \frac{[F][C_0]}{3\varepsilon \quad 5\varepsilon[F]} \tag{2}$$

Samsung Ex. 1010, Page 5 of 13
Samsung Electronics Co., Ltd., et al. v. Molecular Rebar Design, LLC
IPR2025-00356

The fact that $\varepsilon \approx 1$ has been verified previously by reactions performed on reference polymers (e.g., polyvinyl alcohol, PVA – $(-CH_2CH-(OH))_n$) [33].

2.3.3.3.3 Carbonyl groups For the TFH reaction, the measured fluorine and nitrogen atomic concentrations after derivatization ([F] and [N]), as well as the initial atomic concentration of carbon ($[C_0]$), are sufficient to calculate the original concentration of C=O groups present at the surface, using Eq. (3) [33]:

$$[O]_{C=O} = \frac{[F][C_0]}{3\varepsilon \quad 6\varepsilon[F]} \tag{3}$$

The fact that $\varepsilon \approx 1$ has been verified in control studies performed on reference polymers (e.g., polyvinyl methyl ketone, PVMK – $(-CH_2CH-(C(=O)CH_3))_n$) [33].

2.3.3.3.4 Infrared (IR) spectroscopy Attenuated total reflectance-IR (ATR-IR) and transmission IR spectroscopies were used to study functional groups present on MWCNTs. All spectra were acquired using a Mattson Infinity Series FTIR spectrometer with a mercury cadmium telluride detector (4 cm ^{1} resolution). ATR-IR spectra were collected with an attenuated total reflection device (Pike Technologies MIRacle) equipped with a diamond crystal in single reflection mode. Transmission IR spectra were collected from pressed KBr pellets loaded with MWCNT at a concentration of 4 mg MWCNT/400 mg of KBr. All IR spectra represent an average of 500 scans.

2.4. *Structural analysis of MWCNTs*

2.4.1. *Transmission electron microscopy (TEM)*

TEM was performed by dipping a holey-carbon TEM grid into a colloidal suspension of the MWCNTs. Samples were imaged using a Philips CM 300 field-emission gun, transmission electron microscope operating at 297 kV. Images were collected using a CCD camera mounted on a GIF 200 electron energy loss spectrometer.

2.4.2. *Raman spectroscopy*

MWCNT samples were analyzed with a Horiba LabRam HR800 system with a 15 mW 633 nm He–Ne laser with excitation line set to $\lambda = 514.57$ nm and magnification set to 40×. Detailed scans from 300 cm^{-1} to 4000 cm^{-1} were conducted on each MWCNT sample.

3. Results

3.1. *Material assessment*

A complication when studying CNTs is that the quality of the starting materials varies widely among commercial manufacturers, with the most notable difference being the presence of macroscopic amounts of residual amorphous carbon. To verify that the materials we investigated were primarily composed of CNTs, we performed low magnification TEM imaging of MWCNTs both before and after selective oxidative treatments. Results from this analysis are shown in Fig. 4 and reveal, in all cases, that the materials under investigation are predominately MWCNTs. This is in contrast to some MW and many SWCNT materials where the purity of the CNTs available from commercial sources can be less than 50%. It should be noted, however, that almost all commercial sources of CNTs also contain amorphous carbon adsorbed onto the sidewalls. We consider that this type of amorphous carbon to be a component of the CNT and, thus, intrinsic to the surface chemistry of the CNT. More detailed, high magnification TEM images that compare the effect of different oxidative treatments on the MWCNTs structure and surface-bound amorphous carbon content can be found in Section 3.7.

3.2. *Measuring the extent of oxidation*

XPS and EDX were both used to quantify the atomic oxygen concentration following different oxidative treatments. These techniques provide complementary information: XPS is inherently surface sensitive, while EDX is more bulk sensitive. Results from these two techniques are compared in Fig. 5 for all of the MWCNTs analyzed as part of this study. As shown, XPS and EDX results are reasonably well correlated ($r^2 = 0.70$), demonstrating that either technique can provide a measure of oxygen incorporation. The close proximity of the absolute EDX and XPS values is a consequence of the fact that in MWCNTs, like all nanomaterials, a large fraction of the atoms are located at or near to the surface. Fig. 5 also shows that there is a positive, non-zero y-intercept, corresponding to ≈2 at.% oxygen (measured by EDX) for MWCNTs that would be considered "oxygen free" as determined by XPS. This is probably due to oxygen atoms associated with residual iron oxide particles present in the interior of the MWCNT, which would not be detected by XPS. In fact, EDX data shown in Fig. S3 reveals the presence of

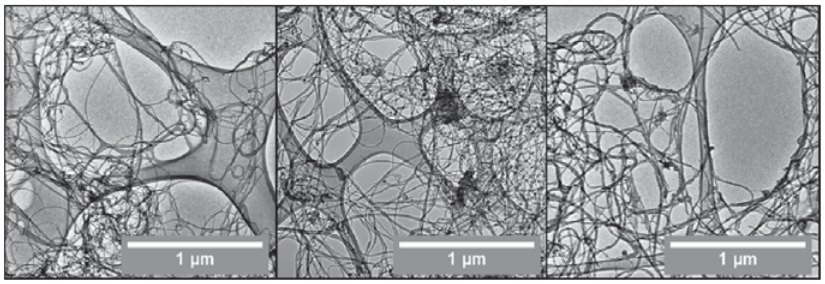

Fig. 4 – Low magnification TEM micrographs (left to right): pristine MWCNTs (0.9% O), O_3 treated MWCNTs (4.7% O), H_2SO_4/HNO_3 treated MWCNTs (10.2% O).

Samsung Ex. 1010, Page 6 of 13
Samsung Electronics Co., Ltd., et al. v. Molecular Rebar Design, LLC
IPR2025-00356

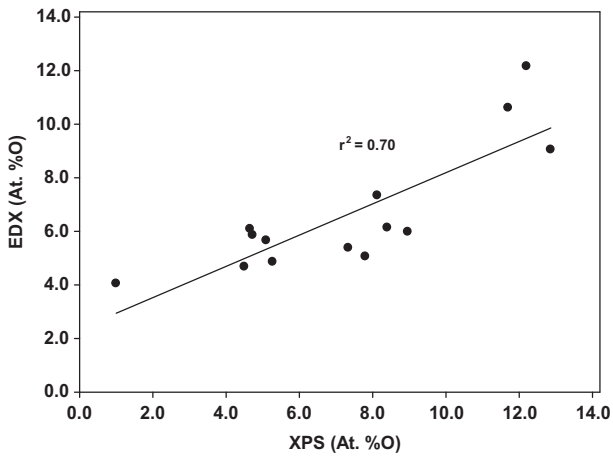

Fig. 5 – Correlation between the at.% O measured by XPS and EDX for both pristine and oxidized MWCNTs.

iron in all MWCNTs studied, in the concentration range of 0.78–0.28 at.%. Fig. S3 also indicates that the imbedded metal nanoparticles are not removed to any significant extent by the oxidative treatments used in the present study based on the lack of correlation between the extent of oxidation and the iron atomic concentration ($r^2 = 0.06$). This inability to remove the internal metal nanoparticles is a consequence of the fact that the effects of the oxidative treatments are dominated by changes to the CNT surface.

In many studies, CNT oxidation is assumed to be localized at the tip ends. A simple geometric calculation reveals that there are ~20 million carbon atoms in a 15 nm diameter MWCNT that has nine walls and is 1 μm long, comparable to the CNTs used in the present investigation. Even if all MWCNTs are open at each end, then only 3000 of the 20 million total carbon atoms are located at the ends. If each carbon atom at the exposed ends is oxidized, this would only correspond to ≈0.0003 at.% oxygen. Based on our XPS and EDX results, this simple calculation demonstrates that the vast majority of the oxygen atoms reside on the CNT sidewalls, likely located at defect sites [47].

3.3. *Influence of commonly used oxidative methods on the extent of MWCNT oxidation*

Among common oxidizing methods (defined by the identity of the oxidant and the reaction conditions) used to treat CNTs, we observed marked differences in the extent of MWCNT oxidation as illustrated in Table 1. The extent of surface oxidation, as measured by XPS, varies from 0.9% for pristine MWCNTs to 10.2% for the H_2SO_4/HNO_3 treated MWCNTs. The most commonly used oxidants/reaction conditions (H_2SO_4/HNO_3, HNO_3, and $KMnO_4$) typically resulted in the highest levels of oxidation (>8%). In contrast, oxidation with H_2O_2, $(NH_4)_2S_2O_8$, and O_3 generally resulted in lower levels of oxidation (4.2–5.1%).

3.4. *Controlling the level of oxidation using w/w% HNO_3*

The easiest and most reliable way to control the extent of MWCNT oxidation was to vary the oxidant concentration,

Table 1 – Extent of MWCNT oxidation after common oxidative treatments.

Oxidative method	Oxidation level (measured by XPS) (%)	Ref.
Pristine ("as received")	~1	n.a.
$(NH_4)_2S_2O_8$	4.5	[41]
H_2O_2	4.5	[39]
O_3	4.7	[40]
20% HNO_3	4.3	[27]
70% HNO_3	9.5	[13]
$KMnO_4$	9.0	[38]
H_2SO_4/HNO_3	10.2	[37]

specifically the w/w% HNO_3 (from 0–70%). Using XPS analysis, the increase in oxidation as the w/w% HNO_3 increases is clearly observed by comparing changes in the intensity of the O(1s) spectral envelope (Fig. 6). The inserts in Fig. 6 also show that the π–π^* shake-up transition, associated with the delocalized π-electrons in CNTs, is attenuated as the level of oxidation increases. The disappearance of this spectral feature for increasingly aggressive reaction conditions can be ascribed to the increased disruption of the π-electron system, indicating a significant change to the electronic structure of the CNT sidewalls. Fig. 6 also highlights the broad and featureless nature of the C(1s) spectral envelope that, even for highly oxidized CNTs, makes meaningful spectral deconvolution extremely difficult.

Fig. 7 shows the effect of varying the w/w% HNO_3 on both the overall atomic oxygen concentration and the distribution of hydroxyl, carbonyl and carboxylic acid groups. The atomic oxygen concentration increases linearly with increasing HNO_3 concentration, while chemical derivatization results indicate that $[O]_{COOH}$ also increases linearly with increasing w/w% HNO_3. Regardless of the oxidant concentration, however, $[O]_{C-OH}$ and $[O]_{C=O}$ groups remains relatively low and constant. Thus, although the level of oxidation can be tuned by varying the w/w% HNO_3, the distribution of surface oxygen functional groups is relatively invariant to the reaction conditions. For HNO_3 treatments, the functional group distribution is determined by the oxidant.

In a related study, Dementev et al. found that, using fluorescent labeling to derivatize hydroxyl, carbonyl and carboxylic acid groups on commercially available SWCNTs that had been oxidized with HNO_3, the concentration of all three functional groups increased compared to the untreated SWCNTs [35]. In contrast to our results, Dementev found that the largest increase in functional groups was associated with the carbonyl groups, although roughly half of the oxygen atoms were present in COOH groups, similar to our results. However, a more direct comparison between these studies is not merited due to differences in the both the detailed oxidizing conditions and the base material (SWCNT *vs.* MWCNT).

3.5. *Influence of the oxidant on functional group distribution*

In Table 1, we compared the effect that different commonly used oxidizing conditions have on the total amount of oxygen imparted to the MWCNTs. However, to compare the effect

Samsung Ex. 1010, Page 7 of 13
Samsung Electronics Co., Ltd., et al. v. Molecular Rebar Design, LLC
IPR2025-00356

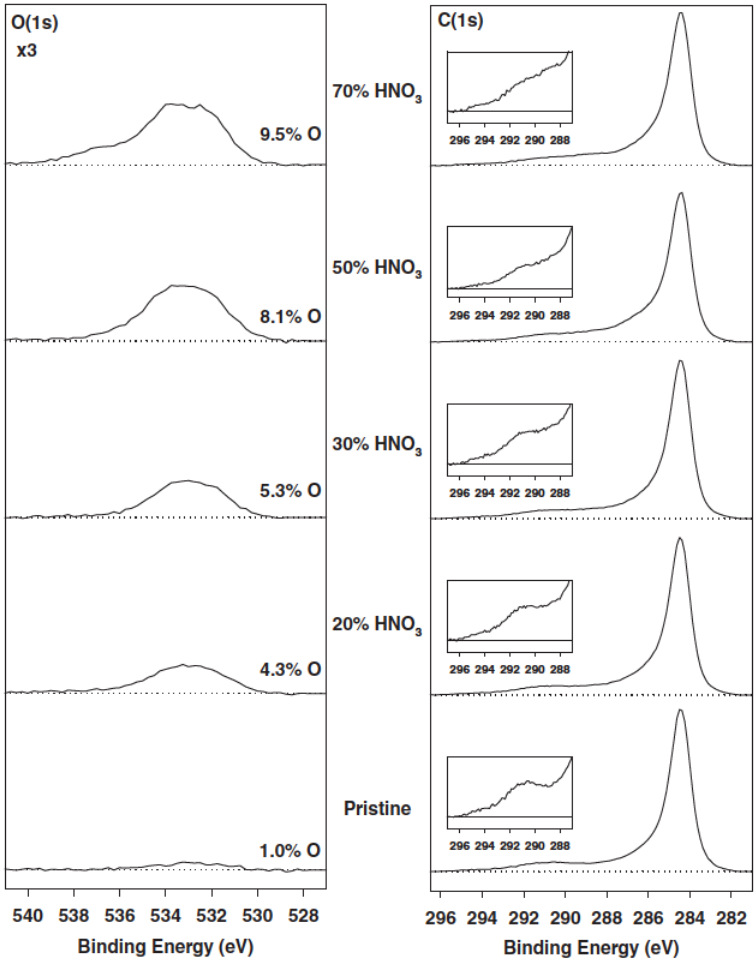

Fig. 6 – C(1s) and O(1s) XPS regions of MWCNTs oxidized by varying concentrations of HNO_3. It should be noted that the O(1s) peaks have been normalized to the accompanying C(1s) peak areas in each case. The insert in the C(1s) region shows the π–π^* transition at ≈291 eV.

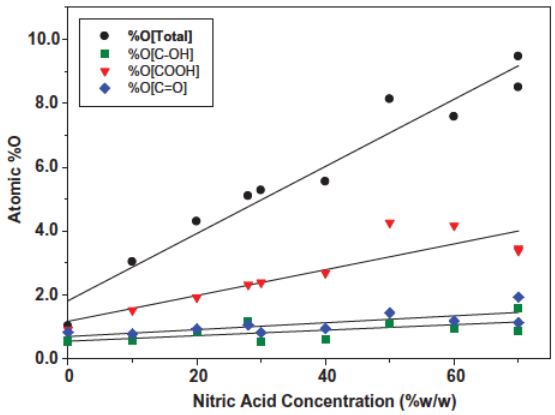

Fig. 7 – Influence of %w/w HNO_3 on the level of oxidation, as well as the distribution of oxygen-containing functional groups.

that different oxidants have on the distribution of oxygen-containing functional groups, we adjusted the reaction conditions by changing the oxidant concentrations in such a way that the overall level of oxidation was comparable (4.5–5.5 at.% O based on integration of the O(1s) and C(1s) spectral envelopes as shown in Fig. 8), irrespective of the oxidant. For example, we oxidized one sample of MWCNTs with 40% HNO_3 and another sample with 87 mg of $KMnO_4$ (as opposed to the normally used 250 mg) to achieve a level of oxidation comparable to that observed with O_3 and H_2O_2 treatments.

Derivatization results for the suite of MWCNTs shown in Fig. 8 are presented in Fig. 9a. These results indicate that the distribution of oxygen-containing functional groups is sensitive to the oxidant with the largest concentration of COOH groups found on $KMnO_4$ treated MWCNTs. Fig. 9a also shows that treatment with either HNO_3 orH_2SO_4/HNO_3 led to similar concentrations of $[O]_{COOH}$, but also a comparatively large fraction of residual (underivatizable) functional groups, such as ethers and esters. In contrast, the H_2O_2 and O_3

Samsung Ex. 1010, Page 8 of 13
Samsung Electronics Co., Ltd., et al. v. Molecular Rebar Design, LLC
IPR2025-00356

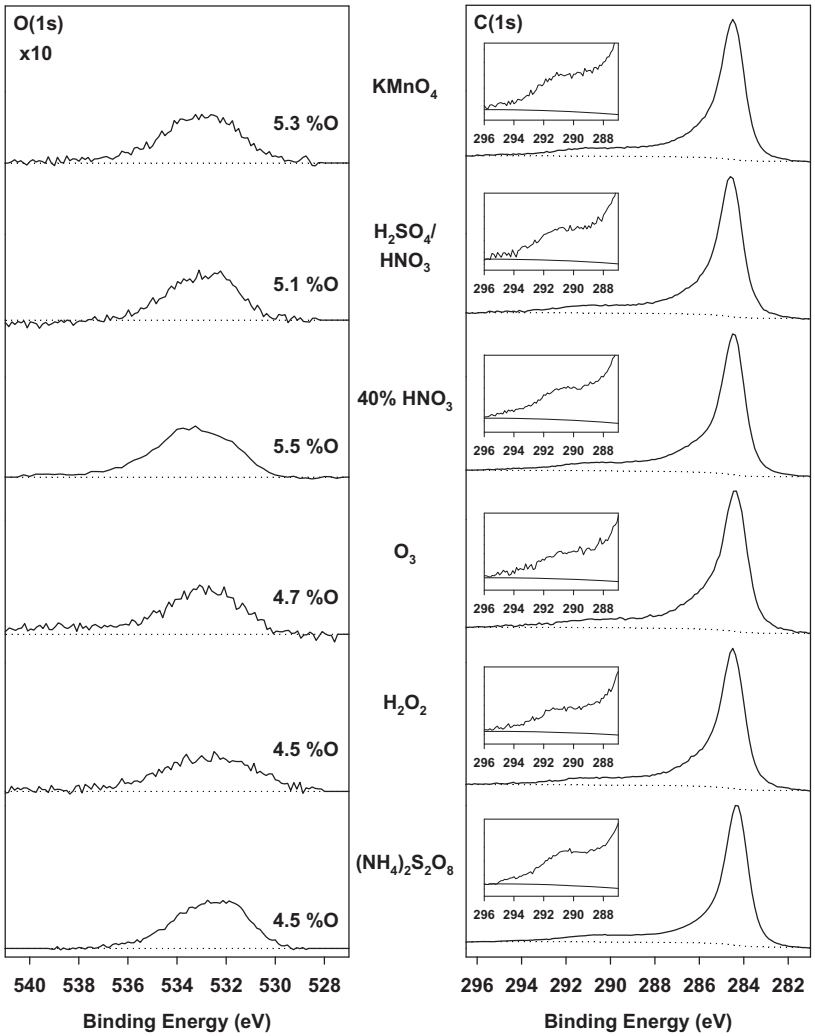

Fig. 8 – C(1s) and O(1s) XPS regions of MWCNTs treated using different oxidants. It should be noted that the O(1s) peaks have been normalized to the C(1s) peak areas in each case. The insets in the C(1s) region shows the π–π^* transition at ≈291 eV.

treatments yielded the smallest concentration of $[O]_{COOH}$, and also produced the largest fractional concentrations of $[O]_{C=O}$ and $[O]_{C-OH}$.

Fig. 9b shows the average fraction of oxygen contained in COOH groups for each of the six different oxidants. We have emphasized the COOH groups due to their importance in attachment strategies [22,44,47–50], rationale functionalization [24,31,51] and in determining environmental properties [30]. For the $(NH_4)_2S_2O_8$, HNO_3, and $KMnO_4$ oxidants the fraction of COOH groups has been measured over a range of reaction conditions by varying the oxidant concentration. Analysis of Fig. 9b reveals that although the fraction of COOH groups among these different oxidants varied by more than a factor of two, the distribution of oxygen-containing functional groups remained relatively constant for a given oxidant, regardless of the reaction conditions. This result is analogous to the one observed for HNO_3 in Fig. 7, and highlights the fact that for a particular oxidant the distribution of oxygen-containing functional groups produced is largely insensitive to the reaction conditions. For the other three oxidants used in Fig. 9b (O_3, H_2O_2, and H_2SO4/HNO_3), multiple batches of MWCNTs were treated under the same oxidizing conditions. Derivatization results plotted in Fig. 9b indicate that there is a large degree of reproducibility in the functional group distribution when the same oxidizing conditions were used on different batches of MWCNTs. The lone exception to this trend was H_2SO_4/HNO_3, where the COOH fraction varied significantly (54 ± 15%) between different MWCNT samples prepared under the same oxidizing conditions. In contrast, the COOH concentration on HNO_3 treated MWCNTs was (46 ± 6%), irrespective of the oxidizing conditions.

A comparison of Table 1 and Fig. 9b also reveals that, in general, the higher $[O]_{COOH}$ concentrations are observed for MWCNTs treated with the most aggressive oxidants (as measured by the maximum amount of oxygen that can be incorporated) such as HNO_3 and $KMnO_4$, while lower $[O]_{COOH}$ and higher $[O]_{C=O}$ are observed for weaker oxidants, such as H_2O_2. In other words, more aggressive oxidants produced a larger fraction of highly oxidized functional groups, in line with the expectations of basic chemical principles.

Samsung Ex. 1010, Page 9 of 13
Samsung Electronics Co., Ltd., et al. v. Molecular Rebar Design, LLC
IPR2025-00356

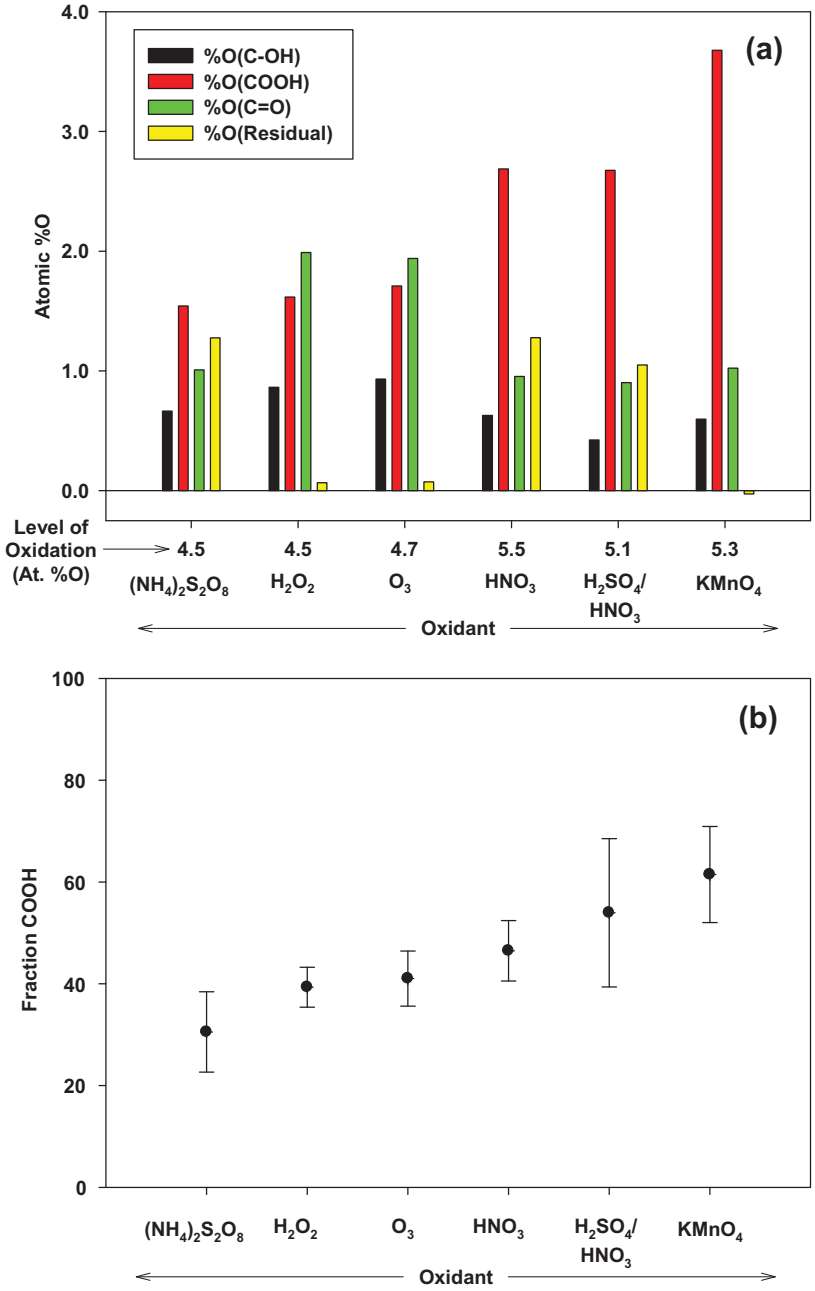

Fig. 9 – (a) Influence of the oxidant on the distribution of oxygen-containing functional groups, measured on MWCNTs that exhibit similar total oxygen concentrations. (b) Average and standard deviation for the percentage of COOH groups measured for each of the six oxidants, using different batches of MWCNTs treated under a range of different reaction conditions. For each oxidant at least three different batches of MWCNTs were treated; for HNO_3 and H_2SO_4/HNO_3, 11 and 9 different batches were used, respectively.

In a previous study using chemical derivatization, we investigated the effect of (HNO_3, O_3, H_2O_2, $(NH_4)_2S_2O_8$) under slightly different reaction conditions (e.g., not refluxing) on another type of BC material, natural char [52]. A comparison of the results from this study with those obtained in the present investigation indicates that the effect of a given oxidant, in terms of the change in atomic oxygen concentration and functional group distribution, is sensitive to the type of BC material. This is perhaps not surprising given the significant differences in structure and initial surface chemistry exhibited by CNTs and chars.

3.6. *IR analysis*

All MWCNTs were analyzed by both ATR-IR and Transmission IR. However, no well-resolved spectral features could be

Samsung Ex. 1010, Page 10 of 13
Samsung Electronics Co., Ltd., et al. v. Molecular Rebar Design, LLC
IPR2025-00356

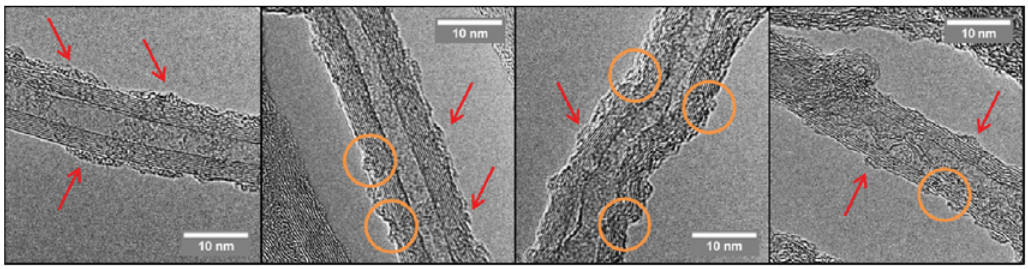

Fig. 10 – Representative TEM Micrographs (left to right): pristine MWCNTs (0.9% O), H_2O_2 treated MWCNTs (4.5% O), H_2SO_4/HNO_3 treated MWCNTs (5.1% O), $KMnO_4$ treated MWCNTs (5.3% O). Amorphous carbon is indicated with arrows, sidewall defects highlighted by circles.

discerned (Fig. S5). In some work with SWCNTs, researchers have found that IR can provide information on the surface functional groups present [47]. However, the added surface functionalities can be difficult to observe at loadings >5% due to contributions from the electronic and intrinsic IR modes of the SWCNT [53]. With MWCNTs, results from the present study and other related investigations of surface oxidation [54] have generally shown that IR spectra are not particularly informative in elucidating surface functionality. Another issue in the IR analysis of CNTs is that vibrational intensity observed at ~3200 cm^{-1} is often erroneously assigned to hydroxyl stretching modes (νOH) associated with surface bound hydroxyl groups rather than water adsorbed onto CNT surfaces [55]. Thus, we have concluded that IR spectroscopy is not an effective technique for identifying the presence or concentration of functional groups on MWCNTs.

3.7. *Effect of oxidative treatments on MWCNT structure*

Raman and TEM were both used to examine the effect of different oxidative treatments on the structure of MWCNTs. From TEM micrographs it is possible to assess the diameter, number of walls, relative concentration of defect sites in the CNT sidewalls, as well as the presence of adsorbed amorphous carbon. Fig. 10 compares representative micrographs of pristine MWCNTs to ones that were exposed to mild (H_2O_2) and aggressive oxidants (H_2SO_4/HNO_3, $KMnO_4$) yet contain a similar amount of surface oxygen (~5 at.%). For the pristine MWCNTs, TEM images show the presence of amorphous carbon wrapped around the MWCNT. In addition, the outermost walls of the MWCNT were long and straight, indicative of a uniform and largely defect-free sidewall structure. Following H_2O_2 treatment, the overall level of amorphous carbon was reduced and a few defects were generated in the sidewall as evidenced by "breaks" in the outermost graphene sheets of the MWCNT. In stark contrast, treatment with H_2SO_4/HNO_3 produced a distortion in the linearity of the MWCNT structure due to damage that, in some cases, extends well beyond the outermost graphene sheet and into the underlying sidewalls. Interestingly, the $KMnO_4$ treated MWCNTs exhibited a larger fraction of COOH groups compared to the other oxidized MWCNTs, yet a relatively low amount of sidewall damage.

Raman spectra of carbonaceous materials exhibit two characteristic peaks at around 1330 cm^{-1} (D-band) and 1590 cm^{-1} (G-band), as shown in Fig. S6 [56]. The G-band is indicative of well ordered structure associated with sp^2 carbon atoms in the graphene sidewalls [56], while the D-band can be caused by either sp^3 carbon atoms at defect sites in the MWCNT sidewalls or amorphous carbon [57]. In principle, the I_D:I_G band ratio can provide a metric of the overall CNT structure; however, this approach is complicated by the adsorbed amorphous carbon that is pervasive in almost all commercial sources of CNTs. Since the oxidative treatments used in this study remove amorphous carbon while simultaneously introducing sidewall defects, I_D:I_G band ratio analysis is ambiguous in terms of the structural information that can be obtained. Consequently, analysis of Fig. S6 reveals little or no correlation between the I_D:I_G band intensity ratio and the oxidant or the extent of oxidation. The one exception is for H_2SO_4/HNO_3 treated MWCNTs where the I_D:I_G band intensity ratio decreases significantly compared to the pristine MWCNTs, presumably a reflection of the effective removal of amorphous carbon from the MWCNT surface, as shown by the TEM image in Fig. 10 (left), despite the extensive sidewall damage. In general, however, our results point to the limitation of Raman in providing unambiguous structural information on the effect of oxidation, unless the pristine CNTs are themselves completely free of amorphous carbon.

To facilitate a direct comparison between different oxidizing conditions, including the effects of different oxidants and reaction conditions, we have restricted the present study to a common source of MWCNTs. Minimally, the degree of surface-bound amorphous carbon is expected to vary between different sources. Regardless, we hypothesize that the qualitative trends observed in the extent of oxidation, functional group distributions, and structural transformation amongst the different oxidative treatments will hold true for other CNTs. However, it is likely that the absolute magnitude of the different chemical and structural changes will be sensitive to the specific CNT under investigation, due to the fact that the intrinsic reactivity of the sidewall carbon atoms is sensitive to the curvature of the CNT [58,59] as well as the defect density.

Samsung Ex. 1010, Page 11 of 13
Samsung Electronics Co., Ltd., et al. v. Molecular Rebar Design, LLC
IPR2025-00356

Acknowledgements

The authors acknowledge financial support from the National Science Foundation (Grant # BES0731147), the Environmental Protection Agency (Grant # RD-83385701-0), and the Institute for Nanobiotechnology (INBT) at Johns Hopkins University. Hanna K. Wilson acknowledges funding from the INBT REU program. The authors would also like to acknowledge the Material Science Department at Johns Hopkins University for use of the surface analysis laboratory, the contributions of Dr. Yo-Rhin Rhim in assisting with heat treatments and Raman spectroscopy as well as Dr. Ken Livi for TEM imaging.

Appendix A. Supplementary material

The supporting information contains three sections: Section S1 includes a full discussion of the TFE/DTBC reaction and characterization of the N-acyl urea surface product which includes one table, one reaction and two figures of NMR data. In Section S2, there is a discussion of the selectivity of the TFE/DTBC reaction towards carboxylic acid groups. Section S3 includes a derivation of Eq. (1). In Section S4, there are three figures on oxidized MWCNTs including EDX, IR, and Raman spectra. Supplementary data associated with this article can be found, in the online version, at doi:10.1016/j.carbon.2010.08.034.

REFERENCES

[1] Spitalsky Z, Tasis D, Papagelis K, Galiotis C. Carbon nanotube–polymer composites: chemistry, processing, mechanical and electrical properties. Prog Polym Sci 2010;35(3):357–401.
[2] Zhang Y, Bai Y, Yan B. Functionalized carbon nanotubes for potential medicinal applications. Drug Discov Today 2010;15(11–12):428–35.
[3] Vaisman L, Marom G, Wagner HD. Dispersions of surface-modified carbon nanotubes in water-soluble and water-insoluble polymers. Adv Funct Mater 2006;16:357–63.
[4] Breuer O, Sundararaj U. Big returns from small fibers: a review of polymer/carbon nanotube composites. Polym Compos 2004(25):630–45.
[5] Wepasnick K, Smith B, Bitter J, Fairbrother DH. Chemical and structural characterization of carbon nanotube surfaces. Anal Bioanal Chem 2010;396(3):1003–14.
[6] Matarredona O, Rhoads H, Li Z, Harwell J, Balzano L, Resasco D. Dispersion of single-walled carbon nanotubes in aqueous solutions of the anionic surfactant NaDDBS. J Phys Chem B 2003;107:13357–67.
[7] Cheng J, Fernando KAS, Veca LM, Sun Y-P, Lamond AI, Lam YW, et al. Reversible accumulation of PEGylated single-walled carbon nanotubes in the mammalian nucleus. ACS Nano 2008;2(10):2085–94.
[8] Chang TE, Jensen LR, Kisliuk A, Pipes RB, Pyrz R, Sokolov AP. Microscopic mechanism of reinforcement in single-wall carbon nanotube/polypropylene nanocomposite. Polymer 2005;46(2):439–44.
[9] Chandra B, Bhattacharjee J, Purewal M, Son Y-W, Wu Y, Huang M, et al. Molecular-scale quantum dots from carbon nanotube heterojunctions. Nano Lett 2009;9(4):1544–8.
[10] Martin CR, Kohli P. The emerging field of nanotube biotechnology. Nature Rev 2003;2:29–37.
[11] Andrews R, Weisenberger MC. Carbon nanotube polymer composites. Curr Opin Solid State Mater Sci 2004;8(1):31–7.
[12] Smith B, Wepasnick K, Schrote KE, Bertele AR, Ball WP, O'Melia C, et al. Colloidal properties of aqueous suspensions of acid-treated, multi-walled carbon nanotubes. Environ Sci Technol 2009;43:819–25.
[13] Smith B, Wepasnick K, Schrote KE, Cho H-H, Ball WP, Fairbrother DH. Influence of surface oxides on the colloidal stability of multi-walled carbon nanotubes: a structure–property relationship. Langmuir 2009;25(17):9767–76.
[14] Rosca ID, Watari F, Uo M, Akasaka T. Oxidation of multiwalled carbon nanotubes by nitric acid. Carbon 2005;43:3124–31.
[15] Esteve W, Budzinski H, Villenave E. Relative rate constants for the heterogeneous reactions of OH, NO_2 and NO radicals with polycyclic aromatic hydrocarbons adsorbed on carbonaceous particles. Part 1: PAHs adsorbed on 1–2 μm calibrated graphite particles. Atmos Environ 2004;38:6063–72.
[16] Vione D, Maurino V, Minero C, Pelizzetti E, Harrison MAJ, Olariu RI, et al. Photochemical reactions in the tropospheric aqueous phase and on particulate matter. Chem Soc Rev 2006;35:441–53.
[17] Song C, Pehrsson PE, Zhao W. Recoverable solution reaction of HiPco carbon nanotubes with hydrogen peroxide. J Phys Chem B 2005;109:21634–9.
[18] Savage T, Bhattacharya S, Sadanadan B, Gaillard J, Tritt TM, Sun Y-P, et al. Photoinduced oxidation of carbon nanotubes. J Phys Condens Matter 2003;15:5915–21.
[19] Datsyuk V, Kalyva M, Papagelis K, Parthenios J, Tasis D, Siokou A, et al. Chemical oxidation of multiwalled carbon nanotubes. Carbon 2008;46:833–40.
[20] Li M, Boggs M, Beebe TP, Huang CP. Oxidation of single-walled carbon nanotubes in dilute aqueous solutions by ozone as affected by ultrasound. Carbon 2008;46:466–75.
[21] Osswald S, Havel M, Gogotsi Y. Monitoring oxidation of multiwalled carbon nanotubes by Raman spectroscopy. J Raman Spectrosc 2007;38:728–36.
[22] Yang D-Q, Sacher E. Strongly enhanced interaction between evaporated Pt Nanoparticles and functionalized multiwalled carbon nanotubes via plasma surface modifications: effects of physical and chemical defects. J Phys Chem C 2008;112:4075–82.
[23] Zschoerper NP, Katzenmaier V, Vohrer U, Haupt M, Oehr C, Hirth T. Analytical investigation of the composition of plasma-induced functional groups on carbon nanotube sheets. Carbon 2009;47:2174–85.
[24] Gromov A, Dittmer S, Svensson J, Nerushev OA, Perez-Garcia SA, Licea-Jimenez L, et al. Covalent amino-functionalisation of single-wall carbon nanotubes. J Mater Chem 2005;15(32):3334–9.
[25] Bergeret C, Cousseau J, Fernandez V, Mevellec J-Y, Lefrant S. Spectroscopic evidence of carbon nanotubes' metallic character loss induced by covalent functionalization via nitric acid purification. J Phys Chem C 2008;112:16411–6.
[26] Hou PX, Bai S, Yang QH, Liu C, Cheng HM. Multi-step purification of carbon nanotubes. Carbon 2002;40:81–5.
[27] Martinez MT, Callejas MA, Benito AM, Cochet M, Seeger T, Anson A, et al. Modifications of single-wall carbon nanotubes upon oxidative purification treatments. Nanotechnology 2003;14:691–5.
[28] Avilés F, Cauich-Rodríguez JV, Moo-Tah L, May-Pat A, Vargas-Coronado R. Evaluation of mild acid oxidation treatments for MWCNT functionalization. Carbon 2009;47(13):2970–5.
[29] Schierz A, Zanker H. Aqueous suspensions of carbon nanotubes: surface oxidation, colloidal stability and uranium sorption. Environ Pollut 2009;157:1088–94.

Samsung Ex. 1010, Page 12 of 13
Samsung Electronics Co., Ltd., et al. v. Molecular Rebar Design, LLC
IPR2025-00356

[30] Cho H-H, Wepasnick K, Smith BA, Bangash FK, Fairbrother DH, Ball WP. Sorption of aqueous Zn[II] and Cd[II] by multiwall carbon nanotubes: the relative roles of oxygen-containing functional groups and graphenic carbon. Langmuir 2009;26(2):967–81.
[31] Maehashi K, Katsura T, Kerman K, Takamura Y, Matsumoto K, Tamiya E. Label-free protein biosensor based on aptamer-modified carbon nanotube field-effect transistors. Anal Chem 2006;79(2):782–7.
[32] Lynam C, Gilmartin N, Minett AI, O'Kennedy R, Wallace G. Carbon nanotube-based transducers for immunoassays. Carbon 2009;47(10):2337–43.
[33] Langley LA, Villanueva DE, Fairbrother DH. Quantification of surface oxides on carbonaceous materials. Chem Mater 2006;18(1):169–78.
[34] Povstugar VI, Mikhailova SS, Shakov AA. Chemical derivatization techniques in the determination of functional groups by X-ray photoelectron spectroscopy. J Anal Chem 2000;55(5):455–67.
[35] Dementev N, Feng X, Borguet E. Fluorescence labeling and quantification of oxygen-containing functionalities on the surface of single-walled carbon nanotubes. Langmuir 2009;25(13):7573–7.
[36] Masheter AT, Xiao L, Wildgoose GG, Crossley A, Jones JH, Compton RG. Voltammetric and X-ray photoelectron spectroscopic fingerprinting of carboxylic acid groups on the surface of carbon nanotubes *via* derivatisation with arylnitro labels. J Mater Chem 2007;17:3515–24.
[37] Blanchard NP, Hatton RA, Silva SRP. Tuning the work function of surface oxidized multi-wall carbon nanotubes via cation exchange. Chem Phys Lett 2007;434:92–5.
[38] Hiura H, Ebbesen TW, Tanigaki K. Opening and purification of carbon nanotubes in high yields. Adv Mater 1995;7(3):275–6.
[39] Peng Y, Liu H. Effects of oxidation by hydrogen peroxide on the structures of multiwalled carbon nanotubes. Ind Eng Chem Res 2006;45:6483–8.
[40] Simmons JM, Nichols BM, Baker SE, Marcus MS, Castellini OM, Lee C-S, et al. Effect of ozone oxidation on single-walled carbon nanotubes. J Phys Chem B 2006;110:7113–8.
[41] Kirk JZ et al. Cutting single-walled carbon nanotubes. Nanotechnology 2005;16(7):S539.
[42] Chiou C-F, Mariñas BJ, Adams JQ. Modified indigo method for gaseous and aqueous ozone analyses. Ozone: Sci Eng: J Int Ozone Assoc 1995;17(3):329–44.
[43] Chilkoti A, Ratner BD, Briggs D. Plasma-deposited polymeric films prepared from carbonyl-containing volatile precursors: XPS chemical derivatization and static SIMS surface characterization. Chem Mater 1991;3(1):51–61.
[44] Bottini M, Tautz L, Huynh H, Monosov E, Bottini N, Dawson MI, et al. Covalent decoration of multi-walled carbon nanotubes with silica nanoparticles. Chem Commun 2005:758–60.
[45] Nakajima N, Ikada Y. Mechanism of amide formation by carbodiimide for bioconjugation in aqueous media. Bioconjugate Chem 1995;6(1):123–30.
[46] Iwasawa T, Wash P, Gibson C, Rebek Jr J. Reaction of an introverted carboxylic acid with carbodiimide. Tetrahedron 2007;63(28):6506–11.
[47] Li X, Niu J, Zhang J, Li H, Liu Z. Labeling the defects of single-walled carbon nanotubes using titanium dioxide nanoparticles. J Phys Chem B 2003;107:2453–8.
[48] Chetty R, Xia W, Kundu S, Bron M, Reinecke T, Schuhmann W, et al. Effect of reduction temperature on the preparation and characterization of Pt–Ru nanoparticles on multiwalled carbon nanotubes. Langmuir 2009;25:3853–60.
[49] Xing Y. Synthesis and electrochemical characterization of uniformly-dispersed high loading Pt nanoparticles on sonochemically-treated carbon nanotubes. J Phys Chem B 2004;108(50):19255–9.
[50] Nakamura T, Ohana T, Ishihara M, Tanaka A, Koga Y. Sidewall modification of single-walled carbon nanotubes with sulfur-containing functionalities and gold nanoparticle attachment. Chem Lett 2006;35:742–3.
[51] Awasthi K, Singh DP, Singh SK, Dash D, Srivastava ON. Attachment of biomolecules (protein and DNA) to amino-functionalized carbon nanotubes. New Carbon Mater 2009;24(4):301–6.
[52] Langley LA, Fairbrother DH. Effect of wet chemical treatments on the distribution of surface oxides on carbonaceous materials. Carbon 2007;45(1):47–54.
[53] Kim UJ, Furtado CA, Liu X, Chen G, Eklund PC. Raman and IR spectroscopy of chemically processed single-walled carbon nanotubes. J Am Chem Soc 2005;127:15437–45.
[54] Yang D-Q, Rochette J-F, Sacher E. Functionalization of multiwalled carbon nanotubes by mild aqueous sonication. J Phys Chem B 2005;109:7788–94.
[55] Kovtyukhova NI, Mallouk TE, Pan L, Dickey EC. Individual single-walled nanotubes and hydrogels made by oxidative exfoliation of carbon nanotube ropes. J Am Chem Soc 2003;125(32):9761–9.
[56] Osswald S, Flahaut E, Ye H, Gogotsi Y. Elimination of D-band in Raman spectra of double-wall carbon nanotubes by oxidation. Chem Phys Lett 2005;402:422–7.
[57] Moonoosawmy KR, Kruse P. Ambiguity in the characterization of chemically modified single-walled carbon nanotubes: a Raman and ultraviolet–visible–near-infrared study. J Phys Chem C 2009;113:5133–40.
[58] Park S, Srivastava D, Cho K. Generalized chemical reactivity of curved surfaces: carbon nanotubes. Nano Lett 2003;3(9):1273–7.
[59] Kausala M, Zhang LC. Deformation-promoted reactivity of single-walled carbon nanotubes. Nanotechnology 2006;17(2):410.

Samsung Ex. 1010, Page 13 of 13
Samsung Electronics Co., Ltd., et al. v. Molecular Rebar Design, LLC
IPR2025-00356